THE JOURNAL OF BIOLOGICAL CHEMISTRY
Vol. 277, No. 46, Issue of November 15, pp. 43682–43690, 2002
Printed in U.S.A.

Mutations within an Intramembrane Leucine Heptad Repeat Disrupt Oligomer Formation of the Rat GABA Transporter 1*

Received for publication, June 6, 2002, and in revised form, September 5, 2002
Published, JBC Papers in Press, September 9, 2002, DOI 10.1074/jbc.M205602200

Petra Scholze, Michael Freissmuth, and Harald H. Sitte‡

From the Institute of Pharmacology, University of Vienna, Währinger Strasse 13a, A-1090 Vienna, Austria

Na^+/Cl^--dependent neurotransmitter transporters form constitutive oligomers, the significance of which is not known. In soluble proteins, leucine heptad repeats drive dimerization; the rat γ-aminobutyric acid transporter GAT-1 (rGAT) contains a motif reminiscent of a leucine heptad repeat in the second transmembrane helix (TM2). We substituted leucine residues in TM2 of rGAT by alanine and tested the ability of the resulting mutants to form oligomers by three methods of Förster resonance energy transfer (FRET) microscopy. Replacement of one leucine (L97A) resulted in considerable loss of energy transfer, replacing two or more ablated it completely. Furthermore, intracellular trapping increased with the number of leucine substitutions. Only rGAT-L97A reached the cell surface to a sufficient amount such that, in intact cells, it was indistinguishable from wild type rGAT with respect to substrate transport, binding of inhibitors, and regulation by protein kinase C. However, in membrane vesicles prepared from transfected cells, all mutants were still functional. In addition, FRET was readily detected during maturation of wild type rGAT, when the bulk of the protein resided in the endoplasmic reticulum. Hence, our findings strongly argue for a role of oligomer formation during biosynthesis and subsequent delivery of the multimer from the endoplasmic reticulum to the plasma membrane.

Na^+/Cl^--dependent neurotransmitter transporters (*e.g.* the transporters for dopamine, serotonin, or GABA)[1] retrieve neurotransmitters from the synaptic cleft into the presynaptic specialization (1). The medical relevance of these proteins is obvious; for instance, it has long been known that antidepressant drugs block the transporter for norepinephrine and serotonin (2). Likewise, tiagabine, an inhibitor of GABA transport, is used as an anticonvulsant in the treatment of epileptic seizures (3). Transporters support bidirectional flux of substrate, *i.e.* not only do they mediate influx of substrate but they also allow for non-exocytotic release of substrate (4). Compounds that induce reverse transport enjoy widespread popularity among illicit drug users; this is particularly true for amphetamine and its congeners, including ecstasy.

Increasing evidence suggests that neurotransmitter transporters are oligomers (5, 6). Constitutive oligomerization has been visualized in intact cells by FRET microscopy (7); the oligomeric nature of neurotransmitter transporters has also been demonstrated by other, more disruptive, approaches, *e.g.* co-immunoprecipitation from detergent extracts and cross-linking (8–10) and by freeze-fracture electron microscopy (11). However, the functional role of oligomer formation remains enigmatic. The hypothesis has been formulated that neurotransmitter transporters function in a manner analogous to ligand-gated ion channels, as binding of substrate induces an ion current (12–14). There is still an ongoing debate whether the GAT operates in a channel-like mode (15, 16) or according to the conservative "alternating access model" (17–19). In the former, binding of substrate induces an ion influx in excess, and in the latter, ions and substrates are translocated with a fixed stoichiometry. Regardless of which model is correct, it is attractive to speculate that the functional transporter unit contains more than one current membrane permeation pathway that allows for concomitant but segregated translocation of substrate and ions (12, 13). A survey of channel structures indicates that oligomers are frequently encountered (20), regardless of whether the channels contain a single pore (*e.g.* K^+ channels and ligand-gated ion channels) or multiple pores (Cl^- channels and aquaporins).

We have therefore searched for mutations that abolish oligomer formation in the rat GABA transporter GAT-1 (rGAT). The rGAT contains a perfect leucine heptad repeat in its second transmembrane helix (TM2); 4 leucine residues (Leu^{83}–Leu^{104}) are separated by 6 intervening amino acids. This leucine heptad repeat conforms to the arrangement found in canonical leucine zippers. Thus, by analogy with transcription factors (21), soluble proteins (22, 23), and soluble domains of membrane proteins (24), TM2 in individual rGAT molecules may drive dimerization by adopting a leucine zipper-like conformation.

Our experiments show that substituting leucine residues by alanine abrogates intermolecular FRET most likely by interruption of oligomer formation in rGAT1. One of those mutants, namely L97A, still binds and transports substrate in a manner indistinguishable from the wild type. Mutations that replace more than one leucine result in intracellular retention of transporters that are still capable of translocating substrate across the bilayer. These data indicate that assembly of rGAT into a stable oligomeric complex is required for export of rGAT1 from the endoplasmic reticulum.

* This work was supported by Austrian Science Foundation/FWF Grants P14509 (to H. H. S.) and P15034 (to M. F.). The costs of publication of this article were defrayed in part by the payment of page charges. This article must therefore be hereby marked "*advertisement*" in accordance with 18 U.S.C. Section 1734 solely to indicate this fact.

‡ To whom correspondence should be addressed: Institute of Pharmacology; University of Vienna, Währinger Str. 13a, A-1090 Vienna, Austria. Tel.: 43-1-4277-64188; Fax: 43-1-4277-9641; E-mail: harald.sitte@univie.ac.at.

[1] The abbreviations used are: GABA, γ-aminobutyric acid; CFP, cyan fluorescent protein; YFP, yellow fluorescent protein; FRET, Förster resonance energy transfer; FRETM, FRET microscopy; DRAP, donor recovery after acceptor photobleaching; SKF 89976A, 1-(4,4-diphenyl-3-butenyl)-3-piperidine-carboxylic acid hydrochloride; rGAT, rat GABA-transporter GAT-1, CMV, cytomegalovirus; TM, transmembrane; AU, arbitrary units; βPMA, phorbol 12-myristate 13-acetate; PKC, protein kinase C; ER, endoplasmic reticulum; wt, wild type.

EXPERIMENTAL PROCEDURES

Site-directed Mutagenesis—The cDNA for the rGAT was a generous gift of Dr. P. Schloss (ZI für Seelische Gesundheit, Mannheim, Germany (25)). The coding region was either subcloned into pRC/CMV (Invitrogen) to create rGAT-pRC/CMV or into pECFP-C1 or pEYFP-C1 (Clontech, Palo Alto, CA) to create CFP-rGAT or YFP-rGAT, respectively, as described previously (7). Mutated versions of rGAT (YFP-rGAT-L97A, YFP-rGAT-L97A/L104A, YFP-rGAT-L83A/L90A/L97A, and YFP-rGAT-L83A/L90A/L97A/L104A) were created by PCR. CFP-rGATΔC and YFP-rGATΔC are truncated forms of rGAT, lacking the last 45 amino acids of the carboxyl terminus. In addition amino acids 827–830 (the last amino acid of transmembrane region XII and the first three of the carboxyl terminus, which are the last four amino acids of the truncated form) were mutated to Ile, His, Arg, and Ile. This mutant was created by fusing the endogenous *Sma*I site formed by amino acids Pro^{825} and Gly^{826} and a second *Sma*I site in the polylinker of pEYFP-C1.

The sequences of all constructs were verified.

Expression of rGAT, Uptake, and Superfusion Assays—Transfections were either performed using the $CaPO_4$ precipitation method or LipofectAMINE Plus™ (Invitrogen). The conditions for propagation of stably transfected HEK-293 cells, uptake, and release assays were as described previously (26).

FRET Microscopy—Ratio imaging and donor photobleaching FRET microscopy were performed at different times after transfection (as indicated in the figure legends) as outlined earlier (7). In brief, A Nikon Diaphot TMD microscope (filter sets: Omega Optical Inc., Brattleboro, VT; CFP filter set: excitation (ex.) 440 nm, dichroic mirror (dichr.) 455 nm, emission (em.) 480 nm; YFP filter set: ex. 500 nm, dichr. 525 nm, em. 535 nm) and a cooled CCD camera (Kappa GmbH, Gleichen, Germany) were used. For ratio imaging FRET microscopy, images were taken with the donor filter set (for CFP) and a FRET filter set (XF88, Omega Optical; ex. 440 nm, dichr. 455 nm, em. 535 nm). Images were captured with both filter sets under identical conditions. Ratio images, which are suited to detect a decrease of donor and an increase in acceptor fluorescence, were calculated by dividing the acceptor filter image by the donor image using NIH image software version 3.02. Photobleaching FRET microscopy was done by continuous illumination for 1 min with a 100-watt mercury lamp and the CFP filter set. During this time interval, images were acquired every 3rd s). This illumination was sufficient to bleach the donor to an extent of less than 20%. Regions of interest were selected over the membrane, and fluorescence emission intensities were quantified using NIH image software. The resulting decay curves were fitted to the equation for a single exponential decay approaching a constant value: fluorescence intensity = $A_0 \cdot e^{-Kt}$ + offset, where A_0 denotes the starting value, offset the final fluorescence signal, and K the decay constant. The photobleaching lifetime constant τ is defined as $1/K$. Different lamps/setups were used over the course of the photobleaching experiments; hence, to allow for comparison, we normalized the τ values by calculating a ratio for each experimental day as follows. The τ value of the fluorescent donor recorded with co-expressed acceptor (τ_{da}) was divided by the τ value of the donor (τ_d) measured in cells expressing the donor only (ratio = τ_{da}/τ_d). In donor recovery after acceptor photobleaching (DRAP) FRET microscopy, a donor image was captured (with a 100× oil immersion objective) using the CFP filter set and a gray filter inserted into the excitation light path to avoid photobleaching of the donor fluorophore. Subsequently, the acceptor was nearly completely bleached by illumination with the YFP filter set (in the absence of the gray filter) for 45 s followed by the acquisition of a second donor image with the CFP filter set and the gray filter using exactly the same CCD camera settings as before. Ratio images of the CFP fluorescence ("after"/"before" acceptor photobleaching) were calculated with the mathematical algorithm of NIH image software (release 3.02). Positive gray values in these ratio images are a clear qualitative indication for FRET, and false positive signals are prevented due to the use of an internal control (*i.e.* the first CFP image).

Imaging and FRET microscopy of maturing rGAT and deletion mutants (all were fused to CFP and YFP) were done on a different microscopic set up. This system consisted of a Zeiss Axiovert 200M inverted epifluorescence microscope equipped with a CoolSNAP fx cooled CCD camera (Photometrics, Roper Scientific, Tucson, AZ). The fluorescence filters used on this setup were purchased from Chroma (Chroma Technology Corp., Brattleboro, VT; CFP filter set: ex. 436 nm, dichr. 455 nm, em. 480 nm; YFP filter set: ex. 500 nm, dichr. 515 nm, em. 535 nm; FRET filter set: ex. 436 nm, dichr. 455 nm, em. 535 nm). Fluorescence images of live cells were taken using the MetaSeries software (release 4.6; both MetaFluor and MetaMorph were used; Universal Imaging Corp., Downingtown, PA). Propagation of captured images was done as outlined above.

Preparation of Membrane Vesicles and Assay for Vesicular Uptake—Adherent cells were washed with PBS (4 °C), detached with a cell scraper, and centrifuged (12,000 × *g*, 10 min, 4 °C). The resulting pellet was resuspended in sucrose buffer (20 mM Tris-HCl, pH 7.5, 1 mM EGTA, 1 mM $MgCl_2$, 0.32 M sucrose) by vigorous vortexing and centrifuged again. The pellet was resuspended in sucrose buffer and sonicated on ice, followed by 10 strokes in a 5-ml glass Dounce homogenizer and subsequently spun down at 18,000 × *g* (60 min, 4 °C). Finally, the membrane vesicles were resuspended in 1 ml of sucrose buffer by sonication and frozen at −80 °C. For GABA uptake, membrane vesicles (30–80 μg/assay) were incubated in 50 mM Tris-HCl, pH 7.5, 1 mM EDTA, 5 mM $MgCl_2$, 150 mM NaCl. In some instances, NaCl was omitted, or its concentration was varied; appropriate concentrations of sucrose were used to maintain iso-osmotic conditions. The reaction (60–80 μl final volume) was started by the addition of [^{3}H]GABA (0.3–30 μM; the specific activity varied between 80 and 0.8 cpm/fmol) and carried out for 0.5–10 min at 20 °C. Uptake was quenched by the addition of ice-cold stop buffer containing 10 mM Tris-HCl, pH 7.5, 1 mM $MgCl_2$, 150 mM NaCl, and 100 μM tiagabine; vesicle-bound radioactivity was trapped on glass fiber filters that were rinsed with 10 ml of ice-cold buffer (10 mM Tris-HCl, pH 7.5, 1 mM $MgCl_2$, 150 mM NaCl, and 10 μM tiagabine). Nonspecific uptake or binding of [^{3}H]GABA was determined in the presence of 100 μM tiagabine or in the absence of NaCl. To account for different expression levels of individual mutants, the amount of YFP-tagged transporter was determined by recording the YFP-specific fluorescence. Membrane vesicles (about 300 μg) where solubilized in 300 μl of sucrose buffer containing 0.5% Nonidet P-40; membranes prepared from non-transfected HEK cells served as control. After 1 h on ice, the insoluble material was removed by centrifugation (1 h at 50,000 × *g*). The supernatant (250 μl) was transferred to a microcuvette (5 × 5 mm), and the fluorescence was recorded in a Hitachi F-4500 fluorescence spectrophotometer; the instrument parameters were set as follows: the slit widths for the excitation and emission monochromator were set at 2.5 nm and the photomultiplier voltage at 950 V. The excitation wavelength was 500 nm; the emission spectrum was recorded between 505 and 600 nm and the peak height determined at 526 nm. The blank was determined with extracts prepared from non-transfected cells; this corresponded to about 18 arbitrary units (AU), whereas the levels of YFP-specific fluorescence ranged from 100 to 700 AU. All recordings were done in parallel.

Chemicals—GF 109203X was from Sigma. Phorbol 12-myristate 13-acetate (βPMA) and 4α-phorbol were obtained from Calbiochem. The source of all other chemicals is listed in Ref. 26. For data calculation, V_{max}, K_m, EC_{50}, and IC_{50} values were calculated using non-linear regression fits performed with Prism (GraphPad, San Diego, CA). The equation used to estimate K_m and V_{max} values was $Y = V_{max} \times X/(K_m + X)$, where $Y = V$ (picomoles per 10^6 cells/min) and X = substrate concentration (moles per liter).

RESULTS

Characterization of CFP/YFP-labeled rGAT-wt and rGAT-L97A—As illustrated in Fig. 1, the second transmembrane domain of rGAT contains a leucine heptad repeat. In order to delineate its possible importance for the formation of oligomeric complexes in rGAT (tagged with CFP or YFP), we replaced the 4 leucine residues with alanine (creating YFP-rGAT-L97A, YFP-rGAT-L97A/L104A, YFP-rGAT-L83A/L90A/L97A, and YFP-rGAT-L83A/L90A/L97A/L104A). We first mutated Leu^{97} alone, because the sequence starting with Leu^{90} is reminiscent of the sequence found in the interacting surface of glycophorin A (LI*XX*GV*XX*; see Fig. 1). If this motif, rather than the leucine heptad repeat, were important for stabilizing the oligomer interface in rGAT, substituting Leu^{97} by alanine ought to be without effect (27). Similar to the wild type rGAT, the mutant rGAT-L97A was present at the plasma membrane (Fig. 2). Interestingly, the fluorescence was not exclusively confined to the plasma membrane; a significantly higher amount of YFP-rGAT-L97A, as compared with YFP-rGAT, was detected within intracellular compartments, presumably in the endoplasmic reticulum and Golgi network (Fig. 2, *A* and *B*, respectively). With all other mutants, the bulk of the protein was trapped within the cells (Fig. 2, *C–E*).

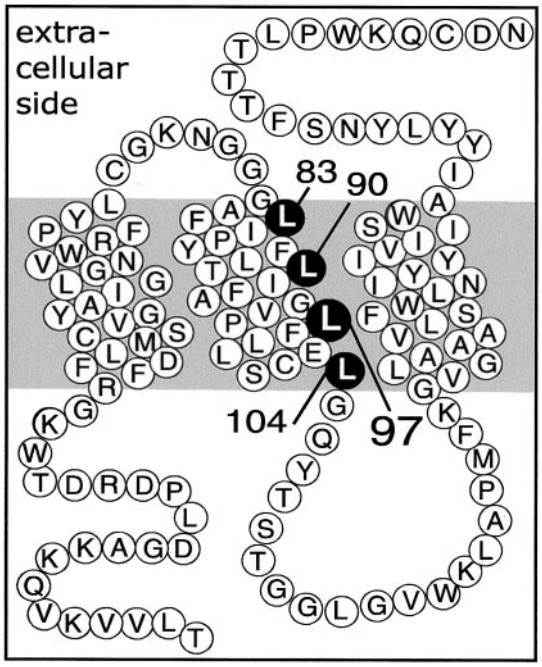

FIG. 1. **Schematic representation of the first three TM segments of rGAT.** The leucine residues in TM2, which were mutated to alanine, are marked in *black*. The *gray box* represents the plasma membrane.

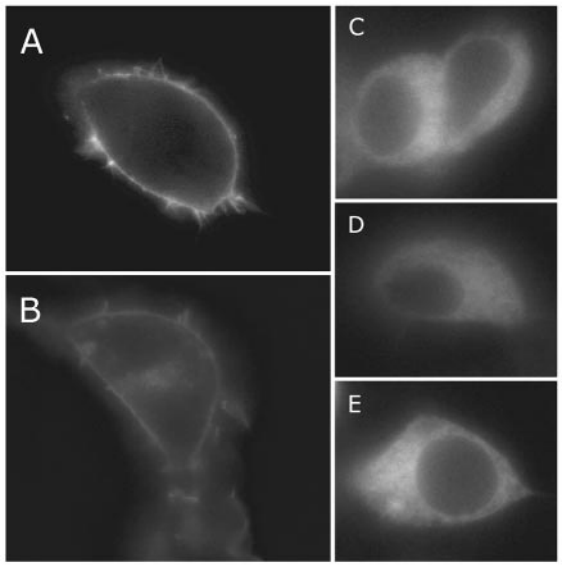

FIG. 2. **Fluorescence microscopy.** HEK-293 cells were transfected with equal amounts of vectors coding for CFP-rGAT and YFP-rGAT (*A*), CFP-rGAT-L97A and YFP-rGAT-L97A (*B*), CFP-rGAT-L97A/L104A and YFP-rGAT-L97A/L104A (*C*), CFP-rGAT-L83A/L90A/L97A and YFP-rGAT-L83A/L90A/L97A (*D*), or CFP-rGAT-L83A/L90A/L97A/L104A and YFP-rGAT-L83A/L90A/L97A/L104A (*E*). The next day, images (63×, oil) were taken using the acceptor filter set. The images are representative of 4–8 transfections each (with 5–10 images/transfection).

Leucine heptad repeats are present within the hydrophobic core of voltage-sensitive K^+, Ca^{2+}, and Na^+ channels; substitutions of leucine residues change the voltage dependence of channel activation and thus presumably affect the opening of the channel upon charge movement (28, 29). Neurotransmitter transporters function in a manner analogous to ion channels because the flux of substrate is accompanied by an ionic current through the transporter (12, 13). It is not known where the ion permeation pathway lies within the transporter protein nor

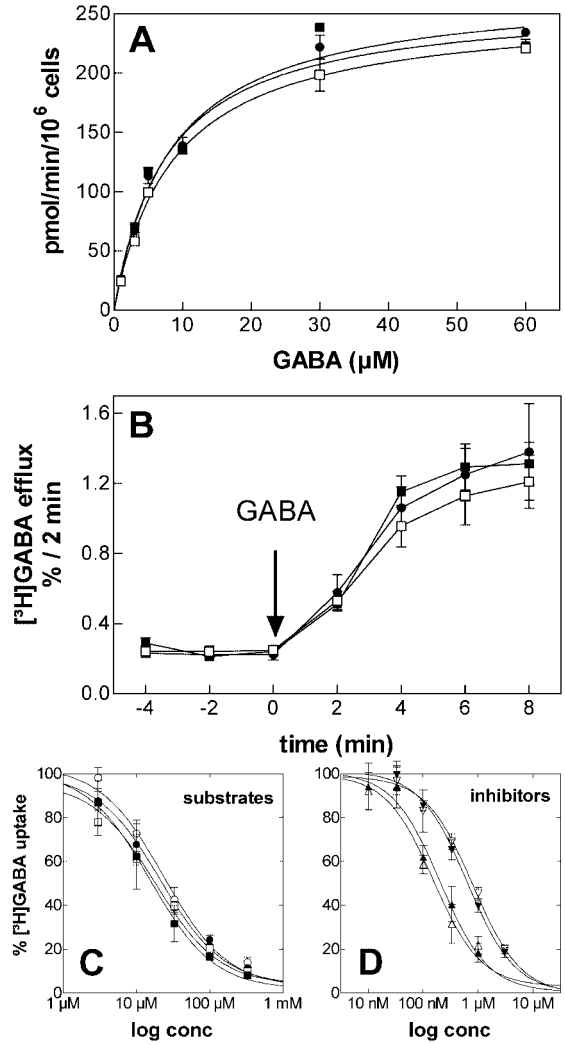

FIG. 3. **Substrate influx (*A*) and efflux (*B*), transport competition (*C*), and inhibition (*D*) in HEK-293 cells expressing YFP-rGAT and YFP-rGAT-L97A.** *A*, cells (5×10^5/well) expressing rGAT (□), YFP-rGAT (■), or YFP-rGAT-L97A (●) were incubated with the indicated concentrations of [^{3}H]GABA for 3 min. *B*, cells (as in *A*) were preincubated with 30 μM [^{3}H]GABA, superfused, and 2-min fractions collected. At the time point indicated (*arrow*), transport reversal was initiated by addition of 30 μM GABA. Fractional efflux is plotted (*i.e.* each fraction is expressed as the percentage of radioactivity present in the cells at the beginning of that fraction). *C* and *D*, cells expressing YFP-rGAT (*closed symbols*) or YFP-rGAT-L97A (*open symbols*) were incubated in 5 μM [^{3}H]GABA for 3 min in the absence (= 100% control) and presence of the substrates (*C*) nipecotic acid (■/□), guvacine (●/○) and inhibitors (*D*) tiagabine (▲/△) and SKF 89976A (▼/▽). Data represent means ± S.E. in at least three independent experiments performed in triplicate.

which segments are involved in translocating the substrate through the bilayer. Accordingly, we verified that mutation of the Leu^{97} to alanine did not interfere with the basic functions of rGAT, namely inward (Fig. 3*A*) and outward transport (Fig. 3*B*). Uptake experiments showed that YFP-rGAT (Fig. 3*A*, ■) and YFP-rGAT-L97A (Fig. 3*A*, ●) transported the natural substrate GABA with K_m values that were virtually indistinguishable (K_m = 7.5 ± 1.1 and 6.3 ± 0.7 μM for YFP-rGAT and YFP-rGAT-L97A, respectively; n = 6) and also identical to the untagged rGAT-wt (Fig. 3*A*, □). Similarly, comparable V_{max} values were obtained (V_{max}, YFP-rGAT-L97A = 97.7 ± 17.2% of V_{max}, YFP-rGAT in six independent, parallel transfections). Likewise, when reverse transport was initiated by challenging [^{3}H]GABA-preloaded cells with unlabeled substrate, YFP-

rGAT (Fig. 3*B*, ■) and YFP-rGAT-L97A (Fig. 3*B*, ●) were indistinguishable from each other and from the untagged rGAT (Fig. 3*B*, □) in their ability to support outward transport. In both cells, expressing YFP-rGAT and YFP-rGAT-L97A, efflux reached a similar plateau after 6 min of drug exposure.

The pharmacological properties of YFP-rGAT-L97A were compared with those of YFP-rGAT. We tested two prototypical substrates (nipecotic acid and guvacine) and two re-uptake inhibitors (tiagabine and SKF 89976A) on the inhibition of [^{3}H]GABA uptake into stably transfected HEK-293 cells. The concentration-response curves were essentially identical (Fig. 3*C*) and IC_{50} estimates similar to those of untagged rGAT (26). Thus, addition of the fluorophore did not affect the basic properties of the transporter, because the affinity for the natural substrate (Fig. 3*A*), the rate of reverse transport (Fig. 3*B*), as well as the pharmacological specificity (Fig. 3*C*) were identical in fluorescent protein-tagged and untagged rGAT.

When uptake was tested in HEK-293 cells expressing YFP-rGAT-L97A/L104A, YFP-rGAT-L83A/L90A/L97A, and YFP-rGAT-L83A/L90A/L97A/L104A, the V_{max} values were barely measurable reflecting their decreased expression on the surface of the cells (*e.g.* V_{max}, YFP-rGAT-L97A/L104A ~10% of rGAT, K_m ~3 μM; $n = 3$, data not shown).

Modulation of YFP-rGAT-wt and YFP-rGAT-L97A by Activation of Protein Kinase C—Many neurotransmitter transporters are subject to inhibitory regulation by PKC; this is also true for rGAT in neurons and glial cells (30, 31). We therefore tested whether the susceptibility to PKC-dependent regulation differed between YFP-tagged rGAT-L97A and wild type YFP-rGAT. Cells expressing either transporter were pretreated with the PKC-activating phorbol ester βPMA for 1 h at room temperature and subsequently allowed to take up [^{3}H]GABA. A preincubation with the inactive phorbol ester αPHR served as vehicle control. Stimulation of PKC decreased V_{max} of [^{3}H]GABA uptake to 52.8 ± 2.2 ($n = 6$) and 59.8 ± 2.8% ($n = 5$) of the control, *i.e.* in cells carrying YFP-rGAT and YFP-rGAT-L97A, respectively. A representative set of saturation hyperbolae that were obtained with transiently transfected cells is shown in Fig. 4*A*. Similar results were obtained in experiments using stably transfected cell lines, and a PKC-dependent decline in V_{max} by ~50% was also observed for the double mutant YFP-rGAT-L97A/L104A (not shown). The reversal of the PKC-dependent inhibition ultimately depends on dephosphorylation and thus presumably relies on the modulation of the transporter by phosphatases (32). We also tested whether wild type YFP-rGAT and YFP-rGAT-L97A differed in their recovery from PKC-mediated inhibition. PKC was deactivated by removing βPMA and by a subsequent 2-h incubation of the cells in the presence of the PKC inhibitor GF109203X. As can be seen from Fig. 4*B*, [^{3}H]GABA uptake recovered to equivalent levels (~75% of the initial V_{max}, which are nearly 90% of the uptake in the presence GF109203X) in cells expressing YFP-rGAT and YFP-rGAT-L97A. Based on these observations, we conclude that an intact leucine heptad repeat is dispensable (i) for binding of substrates and of inhibitors, (ii) for bidirectional transport of substrate through the bilayer, for (iii) modulation of the transporter by regulatory proteins (PKC and phosphatase isoforms).

Oligomer Formation Is Impaired by Mutations in the Leucine Heptad Repeat—We have shown previously (7) that the rat GABA transporter GAT-1 (rGAT) forms oligomers within the plasma membrane. This is illustrated in Fig. 5 where oligomers formed between fluorescently labeled rGAT wt (tagged at the NH_2 terminus with either a CFP or a YFP moiety) were visualized in living HEK-293 cells by ratio imaging, a technique of FRET microscopy that obtains qualitative information. A direct

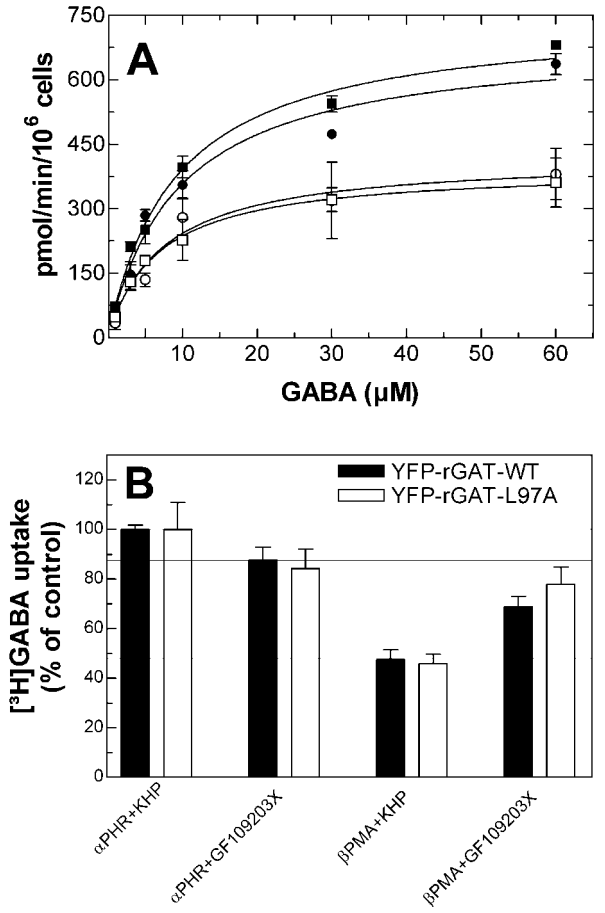

FIG. 4. **Protein kinase C-mediated regulation of YFP-rGAT-wt and YFP-rGAT-L97A.** *A,* HEK-293 cells expressing YFP-rGAT (■/□) or YFP-rGAT-L97A (●/○) were pretreated with 0.2 μM αPHR (*closed symbols*) or with βPMA (*open symbols*) for 1 h and subsequently incubated with the indicated concentrations of [^{3}H]GABA for 3 min ($n = 5$). *B,* cells expressing YFP-rGAT (*closed bars*) or YFP-rGAT-L97A (*open bars*) were pretreated with 0.2 μM αPHR or βPMA for 1 h. Cells were washed twice, treated with either buffer or 25 μM GF109203X for 2 h, and incubated with 60 μM [^{3}H]GABA for 3 min. *Bars* represent means ± S.E. determined ($n = 3$).

protein-protein interaction can be inferred from the decrease of the donor emission (Fig. 5, *1st column, panel CFP filter*) relative to the increase in the acceptor emission (as detected at CFP excitation and YFP emission wavelength; Fig. 5, *1st column, panel FRET filter*). The enhanced emission was demonstrated by calculating the ratio of the two images (shown in Fig. 5, *1st column, panel Ratio image*). Thus, given the additional independent control experiments (see below), the changes in donor and acceptor fluorescence resulted from resonance energy transfer indicating that the two fluorophores were within the Förster distance.

Because YFP-tagged rGAT and rGAT-L97A are indistinguishable when assayed for function or for PKC-mediated regulation, it appears safe to conclude that the overall conformation of rGAT-L97A must be very similar to the wild type conformation. If the leucine heptad repeat was involved in the formation of rGAT oligomers, FRET ought to be absent with YFP-rGAT-L97A. In fact, the fluorescence detected with the CFP filter set exceeded the fluorescence recorded with the FRET filter set (*cf.* top and middle images in Fig. 5, *2nd column*); accordingly, a positive ratio image was barely detectable (Fig. 5, *2nd column, bottom*). We therefore concluded that the removal of a single leucine side chain interfered significantly with the interaction between the CFP/YFP-tagged

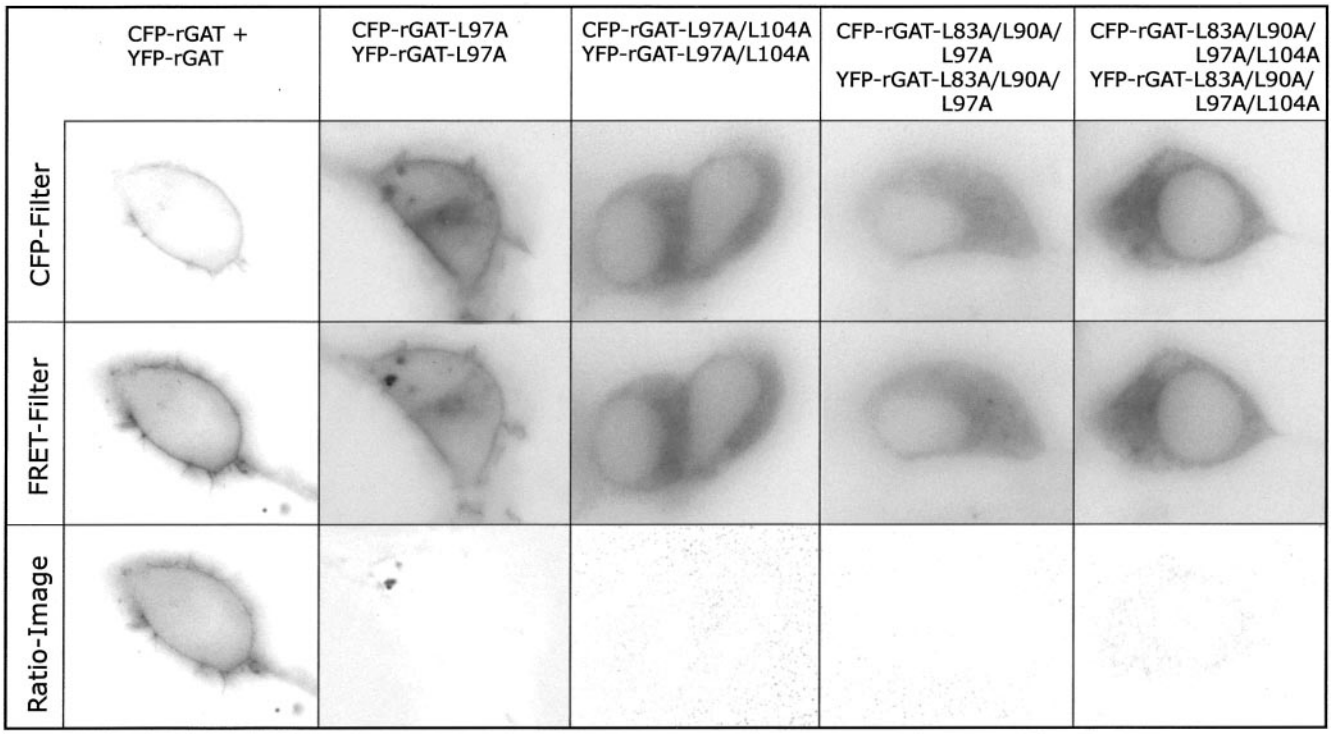

FIG. 5. **Ratio imaging FRET microscopy.** HEK-293 cells were transfected with equal amounts of vectors coding for CFP- and YFP-tagged wild type rGAT or Leu-to-Ala mutants as indicated. The next day, images (63×, oil) were taken using the donor filter set (*CFP filter*) and the FRET filter set (*FRET filter*). The ratio image represents the division of the FRET filter images by the donor filter images using the mathematical algorithm of the NIH image software. The images are representative of 3–6 transfections each (with 5 images/transfection).

amino termini of rGAT-L97A. Accordingly, mutations that replaced more than one Leu by Ala abrogated FRET completely (Fig. 5, *columns 3–5*). This provided additional evidence for the conjecture that the ability of oligomer formation strongly relies on an intact leucine heptad repeat.

Ratio imaging has two limitations. First, donor and acceptor need to be expressed at equivalent levels. The plasmids encoding CFP- and YFP-tagged rGAT-L97A differ by only a few base pairs; hence, provided that identical amounts of each plasmid are employed during transfection, it is very likely that the two proteins are indeed present in similar amounts. Second, the parameters have to be adjusted such that the spurious calculation of a positive ratio image is prevented. This is typically achieved by biasing the recording against YFP fluorescence. Under these conditions, the sensitivity, of our system at least, is too low to reliably detect weak FRET signals. We therefore employed two additional, independent techniques of FRET microscopy, *i.e.* DRAP-FRETM and donor photobleaching FRET microscopy (see also Ref. 7 and 33). Both methods yield valid results even if the concentration of acceptor and donor differ. Contrary to ratio imaging, which directly records the energy transfer, both methods rely on photobleaching; the interaction of a pair of FRET fluorophores within the Förster distance renders the donor less susceptible to bleaching or enhances donor emission upon acceptor bleaching. Obviously, high levels of illumination lead to a rapid decline of either acceptor or donor fluorescence. In the case of DRAP-FRETM, the parameters were set to preserve donor fluorescence while obtaining maximum acceptor bleaching. These conditions were verified using HEK-293 cells transfected with CFP and YFP (where FRET is not to be expected). Images taken with the donor filter set before and after acceptor bleaching show a small decrease in donor fluorescence (Fig. 6*A*, *left column*, note the difference between CFP fluorescence emission *before* and *after*). In contrast, with similar instrument settings, cells that express a concatemer of CFP and YFP (termed CYFP (7)) displayed a robust FRET signal (Fig. 6*A*, *right column*). When DRAP-FRETM was applied to cells transfected with CFP- and YFP-rGAT, we unequivocally observed resonance energy transfer (Fig. 6*B*, *left column*). As predicted from ratio imaging, Förster transfer was almost invisible in rGAT-L97A (Fig. 6*B*, *right column*). Thus, this observation provided further independent evidence for a role of the leucine heptad repeat in supporting oligomer formation.

We confirmed this interpretation by a third approach, namely by donor photobleaching FRETM estimating the time to bleach the donor fluorescence (7). By definition, a resonance energy transfer must have occurred, if the time for bleaching the donor in the presence of the acceptor exceeds that of the donor alone. As an internal standard we again employed CYFP (Fig. 7*A*, ▲) and compared the bleaching kinetics of the CFP moiety to those of CFP that had been co-expressed with YFP (Fig. 7*A*, ▼). It is evident from Fig. 7*A* that the exponential decay curves differed substantially; Fig. 7*B* summarizes the ratios calculated from several experiments. The ratio of τ values (τ_{da}/τ_d) was 1.63 ± 0.1 ($n = 3$) for CYFP, and this was significantly higher ($p < 0.01$, t test) than the ratio obtained with CFP co-transfected with YFP ($\tau_{da}/\tau_d = 1.01 \pm 0.02$). These cytosolic proteins served as tools to gauge our system in the absence and presence of FRET. The dopamine D_2 receptor has been shown to hetero-associate with the somatostatin receptor (34) but not with the human serotonin transporter (7). Thus, as an additional control, we employed the dopamine D_2 receptor (CFP-tagged) together with YFP-tagged rGAT (or mutants thereof). The ratio of τ values obtained in these experiments was 1.02 ± 0.02 ($n = 3$); this proved that the measuring conditions were reliable enough to prevent the spurious recording of FRET over the membrane when no interaction was to be expected. For rGAT, the ratio of τ values was 1.3 ± 0.04 ($n = 4$) and thus clearly indicative of FRET. The value for rGAT-L97A was significantly lower ($\tau_{da}/\tau_d = 1.09 \pm 0.03$, $n = 7$; $p < 0.01$,

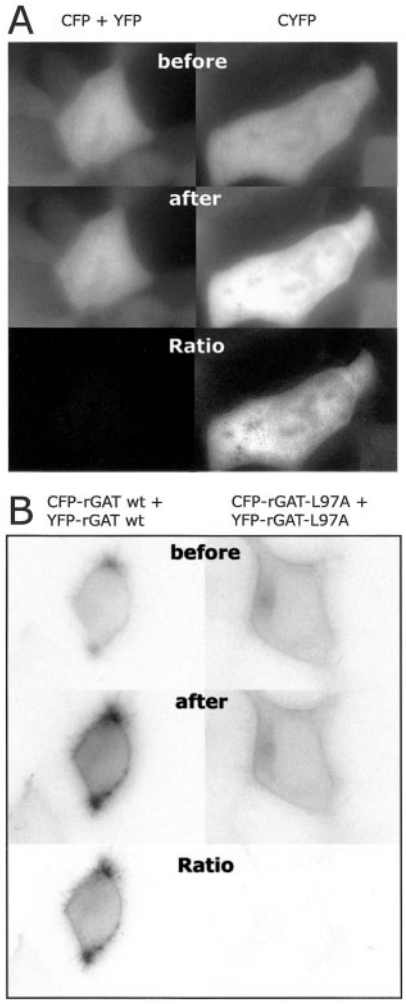

FIG. 6. **DRAP-FRET microscopy.** Two images were taken of cells expressing pairs of FRET donor and acceptor (*A*, *CFP + YFP*, *left*; *CYFP, right*; *B*, *CFP-rGAT + YFP-rGAT*, *left*; *CFP-rGAT-L97A + YFP-rGAT-L97A*, *right*) using the CFP filter-set (100×, oil). To avoid donor photobleaching, the first image (*before*) was taken using a gray filter. Then the acceptor-fluorophore was bleached by exposure (45 s) to intense fluorescence light of 500 nm. Subsequently, the second image was taken using the donor filter set, again in combination with the gray filter (*after*), and a ratio image calculated. The images are representative of four independent experiments.

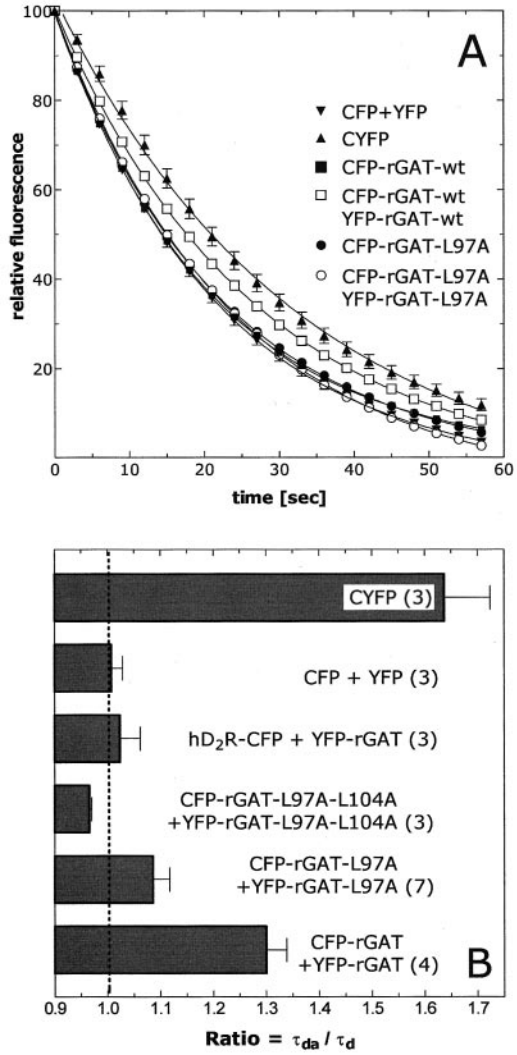

FIG. 7. **Donor photobleaching FRET microscopy.** Cells were transfected with the plasmid encoding CYFP or plasmid combinations encoding CFP + YFP, CFP-rGAT + YFP-rGAT, hD_2R-CFP + YFP-rGAT, CFP-rGAT-L97A + YFP-rGAT-L97A, or CFP-rGAT-L97A/L104A + YFP-rGAT-L97A/L104A or with plasmids encoding only the FRET donor of the combination. The next day, cells were exposed for 1 min to intense light using the donor filter set to selectively induce photobleaching of the donor (63×, oil), and images were captured every 3rd second. Fluorescence intensity was measured in defined regions of the cellular membrane or intracellular regions and fitted to a mono-exponential decay curve to obtain a donor fluorescence lifetime τ. Data in *A* represent means ± S.E. from 10 regions of interest selected from 5 different cells in one experiment. *B*, summary of the lifetime ratios recorded for cells transfected with donor fluorophores with (τ_{da}) or without co-expression of an acceptor fluorophore (τ_d). The number of experiments is indicated in *parentheses*.

one-way analysis of variance and Scheffé's post hoc comparison).

As shown earlier, all mutants other than rGAT-L97A accumulated primarily in an intracellular compartment. Upon transient transfection, rGAT was also visualized in intracellular membrane compartments. Thus, it was possible to test our ability to record FRET over intracellular membranes. We again employed donor photobleaching FRETM and measured the decay of donor fluorescence that was present in the perinuclear area of the cells. The ratio τ_{da}/τ_d amounted to 1.20 ± 0.09 (n = 3). Again, within the intracellular compartment, there was no detectable interaction between rGAT and the control protein, *i.e.* the D_2 receptor (τ_{da}/τ_d = 1.05 ± 0.03; n = 3). Similarly, for rGAT-L97A/L104A (Fig. 7*B*), we obtained a ratio (τ_{da}/τ_d = 0.98 ± 0.02, n = 3) that was not significantly different from 1. This was also true for all other mutants (not shown).

The Mutated Leucine Heptad Repeat Does Not Interfere with Transport Activity—The defective oligomerization of the (Leu → Ala >1) mutants may simply reflect the fact that these transporters fail to fold correctly and that they are therefore retained in the endoplasmic reticulum in an unfolded conformation. Alternatively, oligomerization may be required for efficient export from the endoplasmic reticulum. In order to address this question, we prepared membrane vesicles of HEK-293 cells expressing YFP-rGAT or different Leu-to-Ala mutants (YFP-rGAT-L97A, YFP-rGAT-L97A/L104A, and YFP-rGAT-L83A/L90A/L97A). Under these conditions, all transporters can be exposed to substrate regardless of whether they are retained in intracellular compartments or inserted into the plasma membrane. At high substrate concentrations (20 μM), uptake of [^{3}H]GABA was linear for the first 2 min (Fig. 8*B*, ●). In contrast, at a low substrate concentration (1 μM), the initial rate of transport remained linear for up to >8 min (Fig. 8*A*, ■). This is to be expected for vesicular uptake; because of the limited intravesicular volume, at high substrate concentrations

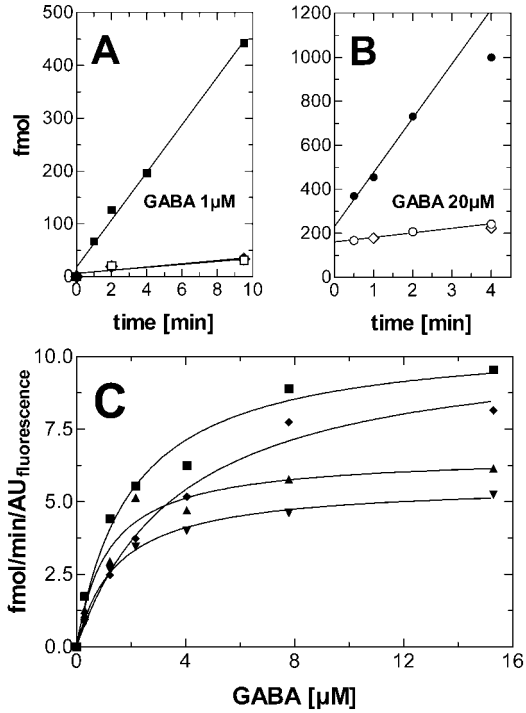

FIG. 8. **Uptake of [^{3}H]GABA by membrane vesicles containing YFP-rGAT, wt and mutants.** *A* and *B*, the time course of [^{3}H]GABA uptake was determined in the presence of 1 (*A*, ■; specific activity 5.5 cpm/fmol) and 20 μM [^{3}H]GABA (*B*, ●; specific activity 1.1 cpm/fmol) using membrane vesicles (29 μg in *A*; 79 μg in *B*) as outlined under "Experimental Procedures." *Symbols* in *A* and *B* represent total uptake of [^{3}H]GABA (■ and ●), uptake in the presence of the GABA re-uptake inhibitor tiagabine (final concentration: 100 μM; □ and ○) or omission of NaCl (♦ and ◇). *C,* membrane vesicles were prepared from HEK-293 cells expressing YFP-rGAT (■), YFP-rGAT-L97A (▲), YFP-rGAT-L97A/L104A (▼), or YFP-rGAT-L83A/L90A/L97A (♦). The vesicles (30–80 μg) were incubated with the indicated concentrations of [^{3}H]GABA at 20 °C for 2 min. Nonspecific uptake/binding determined in the presence of 100 μM tiagabine was subtracted. The transport activity was normalized for YFP fluorescence (*AU*) recorded in detergent extracts prepared from the vesicles. Data are means of duplicate determinations in a single experiment that is representative of three independent experiments.

the amount of [^{3}H]GABA and of co-transported ions ought to saturate rapidly the capacity of the vesicles and thus result in a decline in the transport rate. Furthermore, accumulation of [^{3}H]GABA was reduced upon omission of NaCl (Fig. 8, *A* and *B,* ♦ and ◇) to the levels observed in the presence of the GAT inhibitor tiagabine (Fig. 8, *A* and *B,* □ and ○). Thus, the bulk of [^{3}H]GABA uptake reflected transporter-mediated accumulation. Based on the short linear initial rate, in subsequent experiments an incubation time of 2 min was chosen, and background was determined either in the presence of tiagabine or in the absence of NaCl.

We determined the affinity of wild type rGAT and the individual mutants for the substrate; a set of representative saturation isotherms is shown in Fig. 8*C*. It is evident that there were only modest differences in the apparent affinities for the substrate; the average K_m values (± S.D.; $n = 3$) were 1.23 ± 0.68, 0.97 ± 0.26, 1.05 ± 0.61, and 1.65 ± 0.42 μM for wild type rGAT, YFP-rGAT-L97A, YFP-rGAT-L97A/L104A, and YFP-rGAT-L83A/L90A/L97A, respectively. These K_m estimates are somewhat lower than those estimated for transport in intact cells (K_m ~7 μM; see Fig. 2*A*). This discrepancy, however, can be rationalized if the difference in transmembrane potential is taken into account that exists between intact cells in physiological solutions and vesicular preparations. The membrane potential can also be shown to affect transporters in intact cells (35). Because wild type rGAT as well as the mutants were tagged with YFP, it was possible to correct for differences in expression levels by recording the fluorescence of YFP in detergent extracts that had been prepared from the vesicles. This allowed a quantification of transport capacity in fmol/min/AU. The data in Fig. 8*C* indicate that wild type and mutant transporters do not differ markedly with respect to their V_{max} values. Thus, the reasonably comparable K_m and V_{max} values show that mutations within the leucine heptad repeat do not impede translocation of the substrate across the bilayer.

Intermolecular FRET Was Also Observed in Early Stages of rGAT Maturation in the Endoplasmic Reticulum—Loss of FRET was associated with retention of mutated (but transport competent) versions of rGAT in the endoplasmic reticulum; we surmised that the two phenomena were causally related. In one set of experiments we therefore intended to detect protein-protein interactions at an earlier stage in the maturation of the transporters at the ER level. Thus, we performed comparative donor photobleaching FRETM and DRAP-FRETM (not shown) of co-transfected CFP- and YFP-rGAT as early as 8–10 h and at >24 h after transfection of the cells. It is readily evident that 8 h after transfection, the transporter was almost undetectable at the plasma membrane; the bulk of the protein was still retained at its intracellular sites of synthesis and maturation (Fig. 9*A*, *1st row*). In contrast, at >24 h after transfection, the transporter was predominantly visualized in the plasma membrane in parallel sister cultures (Fig. 9*B*, *2nd row*). Energy transfer was clearly observed in wild type rGAT-containing cells at the early, *i.e.* 8-h, time point; the quantification suggested that this FRET signal was as robust as that recorded over the cell surface of sister cells >24 h after transfection (see τ values in Fig. 9*B*). In the second set of experiments we searched for a mutant that was retained in the intracellular compartment but that still displayed FRET. We identified one such mutant of wild type rGAT in which almost the entire carboxyl terminus was deleted (and was thus termed rGATΔC, lacking 45 amino acids). rGATΔC was trapped within the cell (Fig. 9*A*, *3rd row*); nevertheless, a significant increase in the donor photobleaching time constant was measured in the presence of acceptor (see Fig. 9*B*). Analogous results were obtained with DRAP-FRETM (not shown). This indicated oligomerization of this otherwise retained protein. We did not observe any appreciable difference in the magnitude of the FRET signal between rGATΔC and wild type rGAT either after 8 or 33 h (Fig. 9*B*). Thus, the data provide clear evidence that oligomer formation is detectable at early stages of protein maturation.

DISCUSSION

The mechanisms that support oligomer formation of membrane proteins are still poorly understood, because the forces that stabilize protein-protein interfaces in a hydrophobic milieu differ from those operating in aqueous solution. In the present study, we have focused on the leucine heptad repeat TM2 of the rat GABA transporter-1 and employed three independent techniques of FRET microscopy to investigate its contribution in supporting oligomer formation. Our approach has the advantage that it allows the visualization of protein-protein interactions in the native environment, *i.e.* in the membrane of a living cell. Based on all data sets (ratio imaging, donor photobleaching, and donor recovery after acceptor photobleaching), we conclude that the propensity to form oligomeric complexes is considerably impaired upon substitution of a single leucine residue in TM2 (Leu^{97} by alanine) and completely abrogated by removal of additional leucine side chains. We cannot rule out an overall change in the conformation that would move the amino-terminally attached fluorescent tags in an otherwise

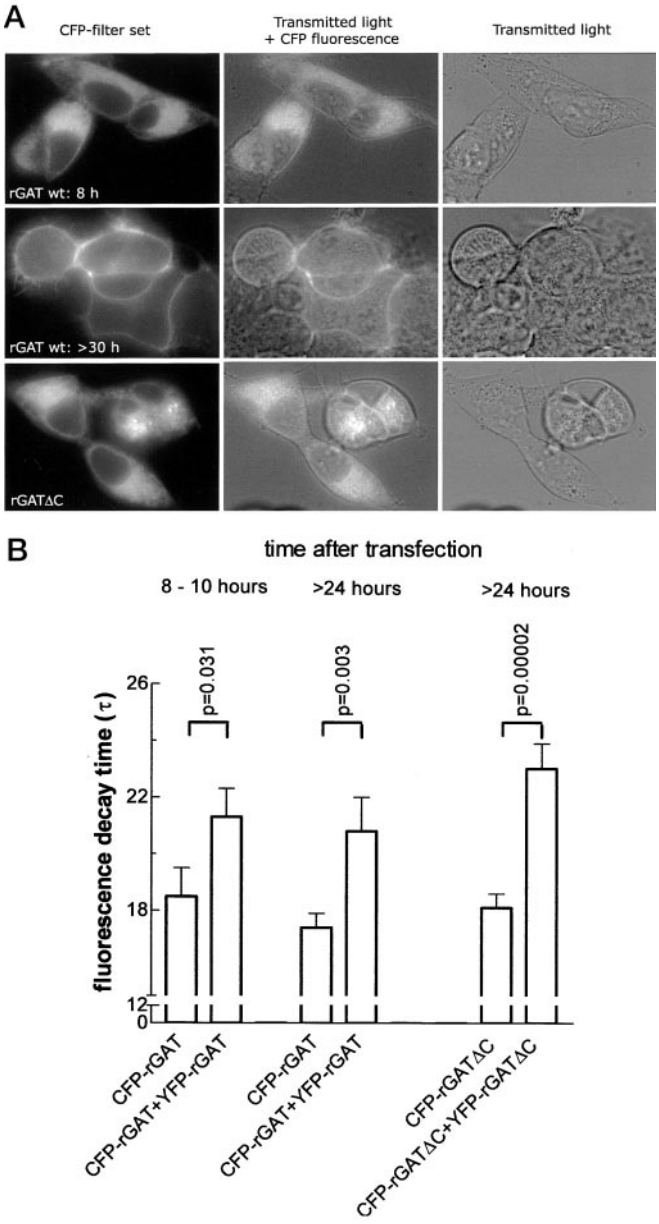

FIG. 9. *A*, HEK-293 cells were transfected with equal amounts of plasmids coding for CFP-rGAT wt and YFP-rGAT wt or with equal amounts of CFP-rGATΔC and YFP-rGATΔC. Images were taken 8 h (*top row*) or 1 day (2*nd* and *3rd row*) after transfection, using the CFP filter set only (*left column*), CFP filter set and transmitted light (*middle column*), or transmitted light only (*right column*). *B*, HEK-293 cells were either transfected with equal amounts of plasmids coding for CFP-rGAT and YFP-rGAT or with CFP-rGAT alone. Experiments were performed 8 h (*left two columns*) or 1 day (*right four columns*) after transfection, as indicated. Cells were exposed to intense light for 1 min using the CFP filter set to selectively induce photobleaching of the donor. Decay of CFP fluorescence intensity was measured in defined regions and fitted to the equation "intensity = $A_0 \cdot e^{-Kt}$" (see "Experimental Procedures"). Fluorescence decay time constant τ is defined as $1/K$. Columns show mean ± S.E. of 15 determinations. Significance of differences was determined by Student's *t* test for independent samples.

intact oligomer beyond the Förster distance (~50 Å). However, the fact that bidirectional transport of substrate, binding of inhibitors, and regulation by protein kinase C was not affected in the mutants (*cf.* Figs. 3, 4, and 8) argues against a global conformational change of this magnitude. The observations are more likely accounted for by a loss in the physical interaction of neighboring amino termini of YFP- and CFP-tagged rGAT-L97A, because their ability to form oligomers is impaired. However, our results obviously do not rule out that the oligomer may be stabilized by interaction of helices other than TM2; in fact, it has been shown that cysteines on top of TM6 can support intermolecular cross-links in the human dopamine transporter (10). Finally, the possibility has to be considered that the effect of the leucine residues is indirect; they may be required for packing of the helices in the hydrophobic core of an individual transporter and thereby indirectly stabilize the interface that supports oligomer formation.

Apart from the current observations, the following three lines of evidence support the assumption that leucine heptad repeats may mediate homophilic interactions of proteins within the membrane: (i) studies of the small protein phospholamban which contains a single transmembrane span (36, 37); (ii) experiments studying the homophilic interactions of single artificial transmembrane segments (38–40); and (iii) a related approach in which the amphipathic segment comprising the leucine zipper of the transcription factor GCN4 was converted into a hydrophobic helix (41). There are, however, several arguments that cast doubt on a role of simplistic extension of the leucine zipper model to membrane proteins, in particular those containing multiple transmembrane domains. First, voltage-sensitive Shaker K^+ channels, for instance, are assembled from identical or related subunits that contain a conserved leucine heptad repeat within their S4–S5 region; these leucine residues, however, are not involved in subunit assembly (28). Similar results have been found for L-type calcium channels, where the heptad motif is thought to play a fundamental role in channel activation rather than helix packing (29). Second, it is difficult to envisage the driving force that would stabilize a leucine zipper in a membrane protein; in aqueous medium helices that contain leucine heptad repeats form a "zipper" because this conformation shields the bulky hydrophobic residue from the aqueous medium. This need to minimize the solvent-exposed surface obviously does not arise in the lipid environment of the membrane. In fact, polyleucine stretches have *per se* little propensity to support helix-helix interactions in a hydrophobic environment (41). The association (as dimers and trimers) is greatly enhanced by hydrogen-bonding donors such as asparagine (39, 41) or aspartate and glutamate (40) in the position "a" of a heptad repeat "$d_n$efgabcd$_{n+1}$," where the positions "d_n" and "d_{n+1}" are held by leucines (or isoleucines), *i.e.* in the helix the hydrophilic residue is sandwiched between two hydrophobic side chains. In this context, it is worth pointing out that a glutamate residue is found in TM2 of all members of Na^+-dependent (monoamine) neurotransmitter transporters. This invariant glutamate (Glu^{101} in rGAT) is found at the a position between two leucine residues (Leu^{97} and Leu^{104} in rGAT, see Fig. 1). It is also worth noting that the constitutive activity of the *neu* oncogene results from a point mutation, which replaces Val^{664} of the Her/erbB2 receptor by glutamate. This substitution results in constitutive (*i.e.* ligand-independent) oligomerization and hence persistent signaling (42, 43).

Based on these arguments, we propose that the leucine heptad repeat and the invariant glutamate in TM2 are important components of the oligomeric interface of rGAT1. The role of Glu^{101} in rat Gat1 is currently being explored. Importantly, we stress, however, that our data do not allow us to draw any conclusions about the structure of the leucine heptad repeat nor about the stoichiometry of transporters in the oligomeric complex. For appropriate synthetic artificial leucine heptad repeats can exist as dimers and trimers (39). In phospholamban, the leucine heptad repeat in the single transmembrane span supports pentamer formation. Obviously, in rGAT (and related transporters) the 12 transmembrane helices impose a space constraint; hence, the number of monomers that can be

recruited into a complex via homophilic association of TM2 is limited. Nevertheless, trimeric complexes can, for instance, readily be envisaged. In addition, as mentioned earlier, there may be additional contact sites that stabilize the oligomer (10).

Our data point to a role of the leucine heptad repeat in supporting the delivery of the transporter from the endoplasmic to the plasma membrane. A role for oligomerization in this process can be inferred from earlier domain swapping experiments in the glucose transporters 1 and 4 (44), and this interpretation is supported by the following observations. Oligomer formation can be observed in the very early stage of rGAT synthesis and maturation. Replacing leucine residues in TM2 interferes with oligomer formation and results in the intracellular retention of (otherwise transport competent) rGAT mutants. These findings suggest that the assembly into a higher ordered complex is indeed important for the export from the ER. However, whereas oligomer formation is necessary, it is clearly not sufficient; resonance energy transfer was similar in magnitude in the carboxyl-terminal deletion mutant rGATΔC and in wild type rGAT. Thus, it is safe to conclude that this mutant existed in oligomeric form. Nevertheless, rGATΔC was not inserted into the plasma membrane. This indicates that an intact carboxyl terminus is also required for ER export. Presumably, the carboxyl terminus represents a docking site for a component of the machinery that recruits rGAT into the budding vesicles and/or targets it to the subsequent compartment. The amino terminus of rGAT is known to bind syntaxin-1A (45), a member of the t-SNARE family; proteins that bind to the carboxyl terminus of rGAT have not yet been identified. In our search for transporters, which are retained in intracellular compartments but have presumably normal transport characteristics, we focused on the carboxyl terminus, because its proteolytic removal does not affect the ability of purified rGAT to transport substrate (46). Truncation of the carboxyl terminus by 38 amino acids reduced V_{max} by 75% relative to cells expressing the full-length transporter (47); the reason for the reduction was not explored, but it may presumably reflect intracellular retention of the truncated transporter. rGATΔC, the mutant investigated in the present work, lacks 45 amino acids; this mutant was not present at the cell surface to any appreciable extent. Conversely, a mutant of rGAT, in which the carboxyl terminus is truncated by 36 amino acids, was delivered to the apical membrane of Madin-Darby canine kidney cells in a manner similar to wild type rGAT (48). The interpretation of our results and those obtained in the earlier two studies is limited by the fact that three different cell types were used. With this obvious caveat in mind, it is possible to postulate that the first 7–9 amino acids immediately adjacent to the last trans-membrane span play an important role in supporting export of rGAT from the ER.

Although the phenomenon of FRET has been known for some 5 decades (49), FRET microscopy has only been applied recently to the study of membrane proteins in living cells. A standard argument raised against this approach is the conjecture that membrane proteins, in particular when heterologously overexpressed, are tightly packed in the bilayer (*e.g.* Ref. 50); this accumulation and the restricted mobility of membrane proteins (often referred to as "membrane crowding") are invoked as a nonspecific source of FRET (thought to support FRET in a nonspecific manner). Our experiments refute this argument in a definitive manner; wild type YFP-rGAT and YFP-rGAT-L97A accumulated to levels in the plasma membrane that allowed for equivalent V_{max} of inward (and outward) transport. Nevertheless, the lack of 9 atoms in YFP-rGAT-L97A sufficed to abolish or greatly blunt resonance energy transfer. This establishes the specificity of FRET microscopy beyond reasonable doubt.

Acknowledgments—We thank Dr. B. R. Binder for providing access to the fluorescence microscope and Dr. J. A. Schmid for invaluable help with FRET microscopy. We are grateful to Dr. U. Gether for helpful comments on the manuscript and to M. Holy and B. Demczuk for excellent technical support.

REFERENCES

1. Rudnick, G., and Clark, J. (1993) *Biochim. Biophys. Acta* **1144,** 249–263
2. Axelrod, J., Whitby, L. G., and Hertting, G. (1961) *Science* **133,** 383–384
3. Iversen, L. (2000) *Mol. Psychiatry* **5,** 357–362
4. Levi, G., and Raiteri, M. (1993) *Trends Neurosci.* **16,** 415–419
5. Klingenberg, M. (1981) *Nature* **290,** 449–454
6. Veenhoff, L. M., Heuberger, E. H., and Poolman, B. (2002) *Trends Biochem. Sci.* **27,** 242–249
7. Schmid, J. A., Scholze, P., Kudlacek, O., Freissmuth, M., Singer, E. A., and Sitte, H. H. (2001) *J. Biol. Chem.* **276,** 3805–3810
8. Jess, U., Betz, H., and Schloss, P. (1996) *FEBS Lett.* **394,** 44–46
9. Kilic, F., and Rudnick, G. (2000) *Proc. Natl. Acad. Sci. U. S. A.* **97,** 3106–3111
10. Hastrup, H., Karlin, A., and Javitch, J. A. (2001) *Proc. Natl. Acad. Sci. U. S. A.* **98,** 10055–10060
11. Eskandari, S., Kreman, M., Kavanaugh, M. P., Wright, E. M., and Zampighi, G. A. (2000) *Proc. Natl. Acad. Sci. U. S. A.* **97,** 8641–8646
12. Sonders, M. S., and Amara, S. G. (1996) *Curr. Opin. Neurobiol.* **6,** 294–302
13. DeFelice, L. J., and Blakely, R. D. (1996) *Biophys. J.* **70,** 579–580
14. Beckman, M. L., and Quick, M. W. (1998) *J. Membr. Biol.* **164,** 1–10
15. Cammack, J. N., and Schwartz, E. A. (1996) *Proc. Natl. Acad. Sci. U. S. A.* **93,** 723–727
16. Risso, S., DeFelice, L. J., and Blakely, R. D. (1996) *J. Physiol.* (*Lond.*) **490,** 691–702
17. Lu, C. C., and Hilgemann, D. W. (1999) *J. Gen. Physiol.* **114,** 445–457
18. Lu, C. C., and Hilgemann, D. W. (1999) *J. Gen. Physiol.* **114,** 429–444
19. Hilgemann, D. W., and Lu, C. C. (1999) *J. Gen. Physiol.* **114,** 459–475
20. Jentsch, T. J. (2002) *Nature* **415,** 276–277
21. O'Shea, E. K., Rutkowski, R., Stafford, W. F., III, and Kim, P. S. (1989) *Science* **245,** 646–648
22. Bartkiewicz, M., Houghton, A., and Baron, R. (1999) *J. Biol. Chem.* **274,** 30887–30895
23. Su, H. P., Brugnera, E., Van Criekinge, W., Smits, E., Hengartner, M., Bogaert, T., and Ravichandran, K. S. (2000) *J. Biol. Chem.* **275,** 9542–9549
24. Bauer, M. F., Sirrenberg, C., Neupert, W., and Brunner, M. (1996) *Cell* **87,** 33–41
25. Sato, K., Betz, H., and Schloss, P. (1995) *FEBS Lett.* **375,** 99–102
26. Sitte, H. H., Singer, E. A., and Scholze, P. (2002) *Br. J. Pharmacol.* **135,** 93–102
27. Fleming, K. G., and Engelman, D. M. (2001) *Proc. Natl. Acad. Sci. U. S. A.* **98,** 14340–14344
28. McCormack, K., Tanouye, M. A., Iverson, L. E., Lin, J. W., Ramaswami, M., McCormack, T., Campanelli, J. T., Mathew, M. K., and Rudy, B. (1991) *Proc. Natl. Acad. Sci. U. S. A.* **88,** 2931–2935
29. Garcia, J., Nakai, J., Imoto, K., and Beam, K. G. (1997) *Biophys. J.* **72,** 2515–2523
30. Beckman, M. L., Bernstein, E. M., and Quick, M. W. (1998) *J. Neurosci.* **18,** 6103–6112
31. Beckman, M. L., Bernstein, E. M., and Quick, M. W. (1999) *J. Neurosci.* **19,** RC9(1–6)
32. Zahniser, N. R., and Doolen, S. (2001) *Pharmacol. Ther.* **92,** 21–55
33. Gadella, T. W., Jr., and Jovin, T. M. (1995) *J. Cell Biol.* **129,** 1543–1558
34. Rocheville, M., Lange, D. C., Kumar, U., Sasi, R., Patel, R. C., and Patel, Y. C. (2000) *J. Biol. Chem.* **275,** 7862–7869
35. Scholze, P., Norregaard, L., Singer, E. A., Freissmuth, M., Gether, U., and Sitte, H. H. (2002) *J. Biol. Chem.* **277,** 21505–21513
36. Arkin, I. T., Adams, P. D., MacKenzie, K. R., Lemmon, M. A., Brunger, A. T., and Engelman, D. M. (1994) *EMBO J.* **13,** 4757–4764
37. Cornea, R. L., Autry, J. M., Chen, Z., and Jones, L. R. (2000) *J. Biol. Chem.* **275,** 41487–41494
38. Gurezka, R., Laage, R., Brosig, B., and Langosch, D. (1999) *J. Biol. Chem.* **274,** 9265–9270
39. Choma, C., Gratkowski, H., Lear, J. D., and DeGrado, W. F. (2000) *Nat. Struct. Biol.* **7,** 161–166
40. Zhou, F. X., Merianos, H. J., Brunger, A. T., and Engelman, D. M. (2001) *Proc. Natl. Acad. Sci. U. S. A.* **98,** 2250–2255
41. Zhou, F. X., Cocco, M. J., Russ, W. P., Brunger, A. T., and Engelman, D. M. (2000) *Nat. Struct. Biol.* **7,** 154–160
42. Weiner, D. B., Liu, J., Cohen, J. A., Williams, W. V., and Greene, M. I. (1989) *Nature* **339,** 230–231
43. Bargmann, C. I., and Weinberg, R. A. (1988) *EMBO J.* **7,** 2043–2052
44. Asano, T., Takata, K., Katagiri, H., Tsukuda, K., Lin, J. L., Ishihara, H., Inukai, K., Hirano, H., Yazaki, Y., and Oka, Y. (1992) *J. Biol. Chem.* **267,** 19636–19641
45. Quick, M. W. (2002) *Proc. Natl. Acad. Sci. U. S. A.* **99,** 5686–5691
46. Mabjeesh, N. J., and Kanner, B. I. (1992) *J. Biol. Chem.* **267,** 2563–2568
47. Bendahan, A., and Kanner, B. I. (1993) *FEBS Lett.* **318,** 41–44
48. Perego, C., Bulbarelli, A., Longhi, R., Caimi, M., Villa, A., Caplan, M. J., and Pietrini, G. (1997) *J. Biol. Chem.* **272,** 6584–6592
49. Förster, T. (1948) *Ann. d. Physik* (*Leipzig*) **2,** 57–75
50. Wilson, M. C., Meredith, D., and Halestrap, A. P. (2002) *J. Biol. Chem.* **277,** 3666–3672